


Data-Driven Inverse Problem for Optimizing the Induction Hardening Process of C45 Spur-Gear

Sevan Garois ^{1,2}, Monzer Daoud ² and Francisco Chinesta ^{1,*}¹ Arts et Metiers Institute, 151 Boulevard de l'Hôpital, 75013 Paris, France; sevan.garois@ensam.eu² French Technological Research Institute for Materials, Metallurgy and Processes (IRT M2P),
4 Rue Augustin Fresnel, 57070 Metz, France; contact@irt-m2p.fr

* Correspondence: francisco.chinesta@ensam.eu

Abstract: Inverse problems can be challenging and interesting to study in the context of metallurgical processes. This work aims to carry out a method for inverse modeling for simultaneous double-frequency induction hardening process. In this investigation, the experimental measured hardness profiles were considered as input data, while the output data were the process parameters. For this purpose experiments were carried out on C45 steel spur-gear. The method is based on machine learning algorithms and data treatment for dealing with inverse approach issues. In addition to the inverse modeling, a forward problem-based verification completes the study. It was found that according to promising results that this method is suitable and applicable for inverse problem of hardness modeling.

Keywords: inverse problem; machine learning; induction hardening; C45 steel; spur-gear



Citation: Garois, S.; Daoud, M; Chinesta, F. Data-Driven Inverse Problem for Optimizing the Induction Hardening Process of C45 Spur-Gear. *Metals* **2023**, *13*, 997. <https://doi.org/10.3390/met13050997>

Academic Editor: João Manuel R. S. Tavares

Received: 19 April 2023

Revised: 15 May 2023

Accepted: 18 May 2023

Published: 21 May 2023



Copyright: © 2023 by the authors. Licensee MDPI, Basel, Switzerland. This article is an open access article distributed under the terms and conditions of the Creative Commons Attribution (CC BY) license (<https://creativecommons.org/licenses/by/4.0/>).

1. Introduction

Induction hardening (IH) is a heat surface treatment process that is widely employed in various industries, such as aerospace and automotive, to improve the mechanical properties of workpieces [1,2]. The process begins with a powerful induction heating, followed by a rapid quenching step. It has the advantage of providing rapid and localized surface heating of the desired areas without affecting the metallurgy of the bulk material, as well as good reproducibility [3]. As a result, a fine-grained martensite phase [4–6] and a compressive residual stress field [7–9] are induced in the surface layer, which enhances the fatigue life behavior of engineering components [10,11]. However, high temperatures coupled with longer heat time could lead to grain growth (causing a degradation in fatigue strength), data scatter, and excessive gear distortion [12,13]. Accordingly, the control of the process parameters is highly important to validate the effectiveness of this heat treatment process [14]. This type of investigation is known as the forward approach.

In the inverse approach, the goal is to determine the cause of a given effect, or to reconstruct an unknown quantity from observations or measurements [15]. This approach is often regarded as a critical and challenging issue for physics, science, and engineering. In fact, it requires making assumptions and using mathematical models to estimate the unknown parameters that are responsible for the observed data. Moreover, it often involves non-unique solutions and high computational power demands. Inverse problems can be found in many fields such as computer vision and imaging [16–20], vibration mechanics [21], electromagnetic [22] medicine [23,24], groundwater modeling [25], and machine learning [26,27]. When the solution to such problems is not unique or sensitive to small perturbations in the data, they represent ill-posed problems. These problems are usually more difficult to solve than well-posed problems and require additional assumptions or regularization to obtain a unique and stable solution.

Concerning the forward problem, a significant amount of research works has been conducted to study the IH process [28–34]. While experimental approaches can provide

valuable insights [35], they can be time-consuming and have limitations in terms of the range of validation. A more efficient method for guiding and optimizing processes is the use of numerical techniques, such as finite element modeling (FEM), which has proven to be relevant in dealing with multiphysics-based parametrized problems [36]. As a result, many studies have focused on using FEM to analyze hardness with relevant accuracy [37–43]. However, this approach is restricted by the computational cost. Hence, machine learning algorithms have been recently employed. They tend to reduce computational time while maintaining accuracy in the modeling of parameters of interest such as hardness and residual stress [38,44–46].

In the context of an inverse problem, fewer studies have been conducted for IH. They are related to the estimation of the power levels using the temperature as input in steel cylinders [47] and the heat transfer coefficient using the surface temperature in a steel billet [48]. In industry, solving the inverse problem for IH can have a number of benefits. Some of the main goals include improving efficiency by determining the optimal input parameters to meet the technical specifications for a given workpiece, reducing the amount of time and resources required to produce a desired output, and improving efficiency and precision. Moreover, it allows more flexibility in the hardening process, making it possible to treat different workpieces or geometries.

This work proposes to study the induction hardening process with inverse problem approach. The inverse problem can be defined as follows: Let A and B be two spaces and $f : A \rightarrow B$ an operator. Consider the equation

$$f(p) = h \quad (1)$$

where $h \in B$ is the exact datum. Finding the function f satisfying the above equation, given f and h , is the inverse problem associated to Equation (1). In the present case, A and B should be the space of the induction process parameters and the space of hardness, respectively. Inverse problems can be solved using a variety of mathematical techniques such as optimization [49,50], regularization [51–53], Bayesian inference [54–56] and machine learning algorithms [57,58]. In this work, a simple method based on machine learning is presented to solve the problem expressed by Equation (1). Section 2 presents the experiments from which the data are collected. Section 3 is dedicated to the definition of the inverse problem in the context of induction hardening. Section 4 shows the results and the validation through the forward problem.

2. Experimental Details

The series of induction hardening experiments under simultaneous double-frequency is performed on C45 steel spur-gears. The gear data was summarized in Table 1, while the process parameters were listed in Table 2. During these experiments, gears were mounted on a rotating chuck. The heating phase was performed by using a rectangular shape inductor of 12.25×20 mm having an air-gap of 2 mm, while the subsequent cooling shower of a polymer–water mixture was applied by another coaxial ring as shown in Figure 1. The temperature on the surface at the tooth root was measured using an Optris pyrometer. Micro-hardness Vickers (HV0.3) profiles were conducted in the normal direction to the surface of the gear at the tooth tip and root and on a transversal section, according to ISO 6507 norm [59], to determine the penetration hardening at these two locations.

Table 1. Main characteristics of the treated gear.

Module	No. of Teeth	Width	Addendum Circle	Pitch Circle	Root Circle
2.5	22	10 mm	60 mm	55 mm	48.75 mm

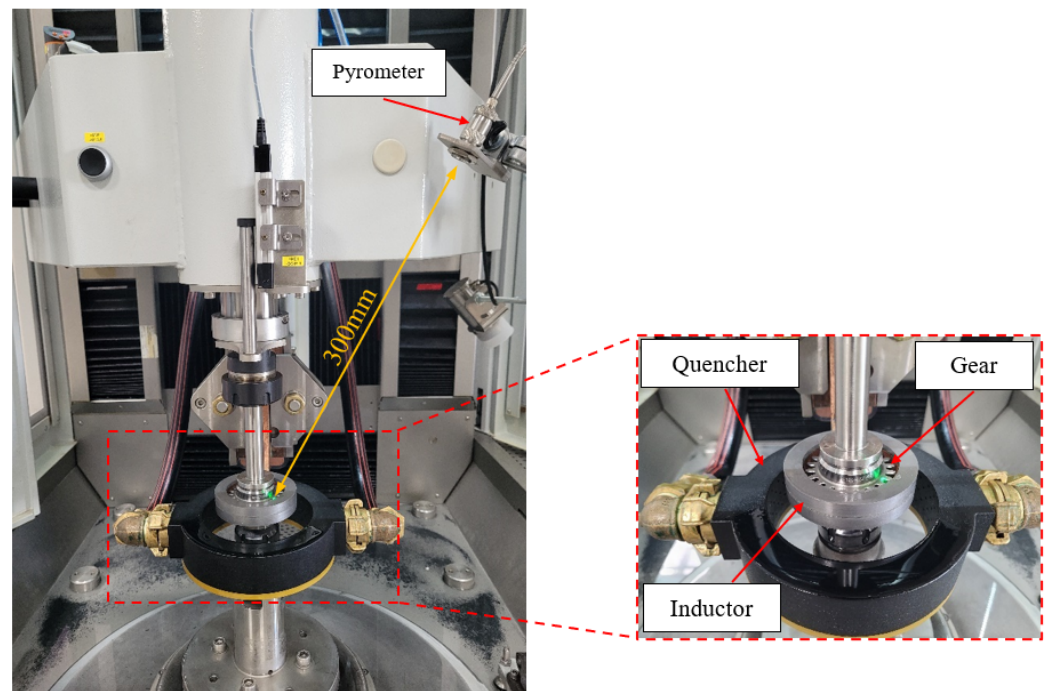


Figure 1. Experimental double-frequency induction hardening setup.

Table 2. Induction heat treatment conditions.

Run #	Medium Frequency	High Frequency	Power of HF	Power of MF	Time	Temperature
	MF (kHz)	HF (kHz)	P_{HF} (kW)	P_{MF} (kW)		
1	13	256	143	88	0.17	780
2	12	258	225	138	0.17	1080
3	12	258	225	138	0.2	1200
4	12	257	143	113	0.17	835
5	12	258	184	113	0.17	935
6	12	258	225	113	0.17	1005
7	13	257	143	113	0.2	×
8	13	257	184	88	0.2	917
9	13	257	184	138	0.24	1189
10	13	257	143	138	0.2	1059
11	12	257	184	113	0.2	1025
12	13	257	184	88	0.24	1028
13	12	258	225	88	0.2	999
14	13	257	143	88	0.24	925
15	12	258	225	113	0.24	1167
16	12	258	225	88	0.17	900
17	12	257	184	138	0.17	1005
18	13	257	143	113	0.24	1039
19	13	257	143	138	0.24	1145
20	12	258	225	138	0.24	1217
21	12	258	225	88	0.18	884
22	12	258	198	134	0.17	920
23	×	×	238.5	94	0.17	890
24	×	×	247.5	98	0.19	958
25	12	257	202	110	0.17	884
26	×	×	175.5	102	0.19	889
27	12	257	202.5	118	0.17	887

Table 2. Cont.

Run #	Medium Frequency	High Frequency	Power of HF	Power of MF	Time	Temperature
	MF (kHz)	HF (kHz)	P_{HF} (kW)	P_{MF} (kW)	t (s)	T (°C)
28	×	×	193.5	102	0,19	876
29	×	×	238.5	88	0.19	906
30	×	×	247.5	88	0.19	905
31	×	×	247.5	94	0.17	858

×: missing values.

3. Inverse Problem

An inverse problem is the process of calculating from a set of observations the input parameters that produced them. Hence, in the present case, the measured hardness profiles should be set as input in a machine learning algorithm to predict the process parameters.

3.1. Hardness Profile Treatment

Based on the collected experimental data, the space X of available variables can be defined as:

$$X = \{MF, HF, P_{MF}, P_{HF}, T, d, t, H\} \quad (2)$$

where MF and HF are the medium and high frequency, respectively, P_{MF} and P_{HF} are their respective generator powers, T is the temperature measured at the surface close to the tooth root, d is the depth at which the hardness was measured, t is the heating duration, and H is the measured hardness. Frequencies being almost constant, they can be excluded. Hence, the studied space of variables reduces to:

$$X = \{P_{MF}, P_{HF}, T, d, t, H\} \quad (3)$$

The process parameters are the time and generator powers P_{MF} and P_{HF} . Hence, the problem can be described as finding a model f such as :

$$f(H) = (t, P_{MF}, P_{HF}) \quad (4)$$

There are 31 runs as listed in Table 2 composed of 60 hardness measurement point each. Hence, the hardness set as input, there are as many input variables such as:

$$f(H_1, H_2, \dots, H_{60}) = (t, P_{MF}, P_{HF}) \quad (5)$$

However, it is preferable to have fewer variables than data points [60,61] to allow the use of linear algorithms for modeling. It was previously shown that it is efficient to encode a profile as a few variables [38]. This procedure has the advantage of standardizing the profile to a fixed number so that any new profile would be treated equally and avoid data shape problems. Hence, in this work, each hardness profile is encoded as 5 characteristic points. The first point H_0 is at a depth of 3 μm . The second and third ones H_1 and H_2 correspond to the hardness measurements localized at 1/3 and 2/3 of the total depth, respectively. Then, $H_{0.8}$ is the hardness at the conventional depth such that $H_{0.8} = 0.8 \times H_0$. The last one H_3 is the last measured point of the profile which corresponds to the bulk hardness. Some profiles with their selected hardness points are illustrated in Figure 2.

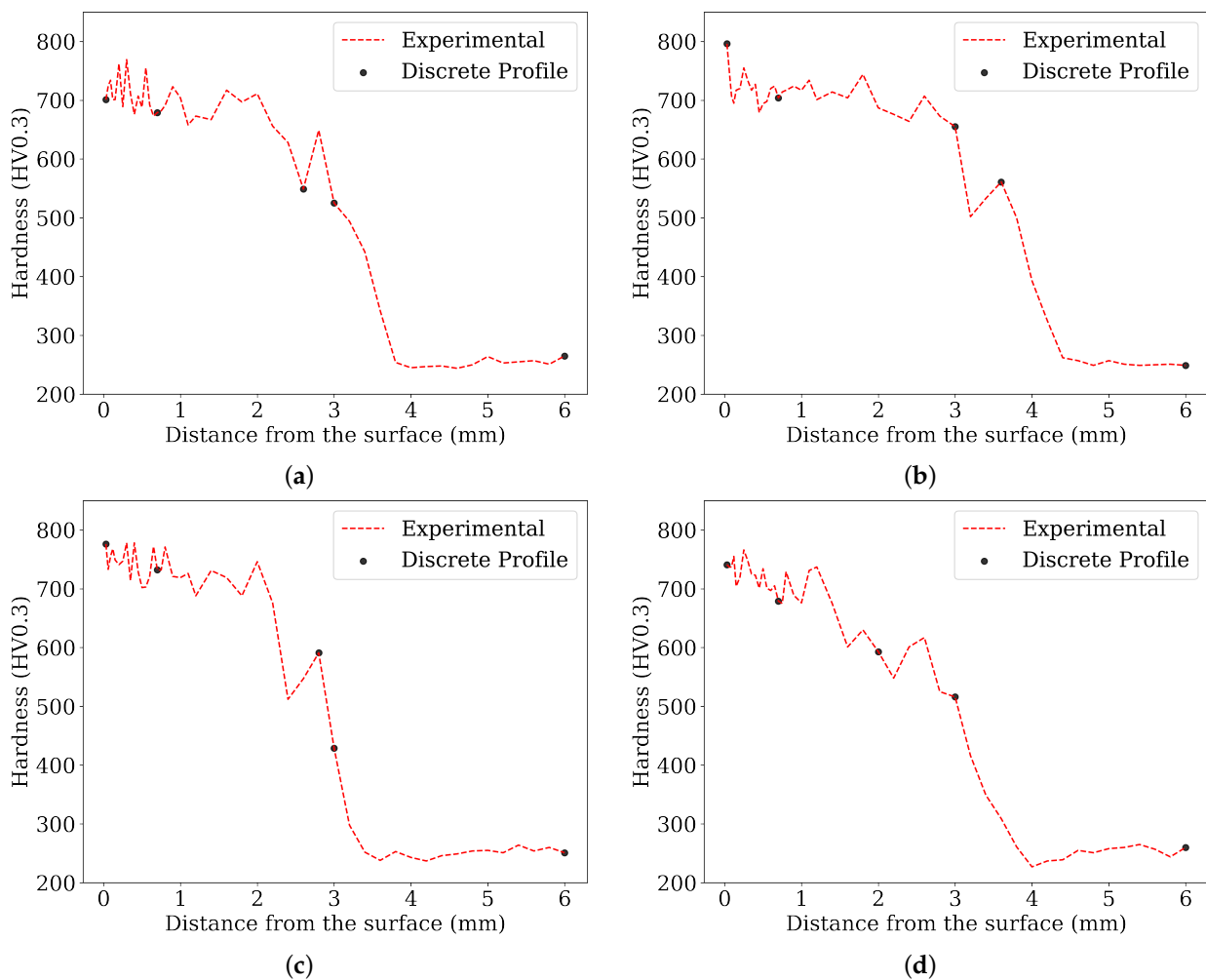


Figure 2. Selected hardness points from the measured hardness profiles. (a) Run #2; $T = 1080\text{ }^{\circ}\text{C}$; (b) Run #12; $T = 1028\text{ }^{\circ}\text{C}$; (c) Run #22; $T = 920\text{ }^{\circ}\text{C}$; (d) Run #30; $T = 905\text{ }^{\circ}\text{C}$.

Then, H can be decomposed as:

$$H = \{H_0, H_1, H_{08}, H_2, H_3\} \tag{6}$$

The inverse problem can be now written as:

$$f(H_0, H_1, H_{08}, H_2, H_3) = (t, P_{MF}, P_{HF}) \tag{7}$$

3.2. Experiencing the Ill-Posed Problem

The inverse problem encounters a major issue. A combination of the output parameters into one should be a solution. Indeed, hardness depends on temperature history, it is the product of the power of generators P_{HF} and P_{MF} and the time t . To prove the non-uniqueness of a solution, considering an artificial neural network (ANN) as f in Equation (7), known as a universal function approximator, which means that, theoretically, it can learn any mathematical function, regardless of its complexity [62]. Moreover, as a global estimator, if a solution exists, a sufficient number of iterations (epochs) during the training should let the ANN converge to it. An ANN with three hidden layers all composed of 120 neurons was built, and a dropout layer to ensure avoiding overfitting [63] was added to the neural architecture. The ANN was trained on several different hyperparameters and number epochs to reach convergence.

The results of the ANN are almost constant for each target variables as illustrated in Figure 3. Moreover, the ANN doesn't converges to a unique solution, as seen in the

evolution of the training phase shown in Figure 4, which confirms the absence of a unique solution.

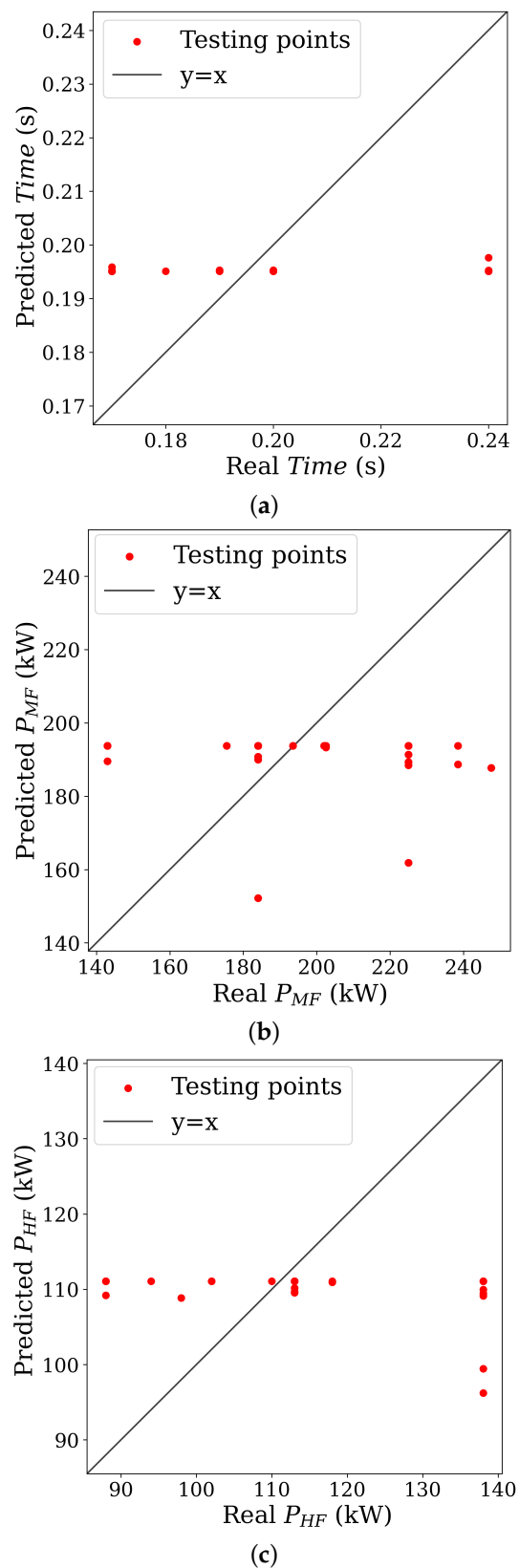


Figure 3. ANN process parameters predictions. (a) time (s); (b) and (c) power generator in medium and high frequency, respectively.

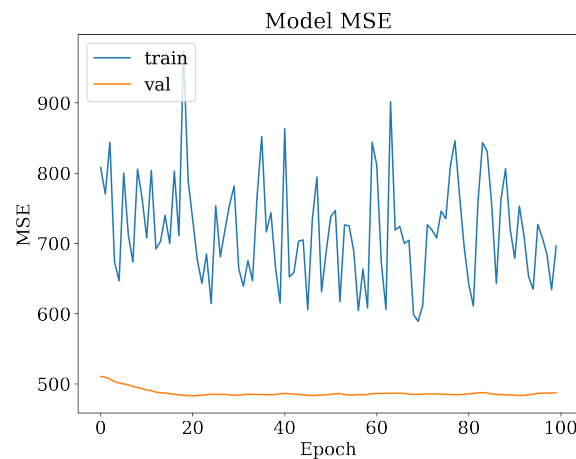


Figure 4. Training (train) and validation (val) error with respect to the epoch (iteration of training).

3.3. Physics-Informed Inverse Problem

In this inverse problem, the output parameters are the powers P_{HF} , P_{MF} , and time t . As mentioned above, the major issue is the difficulty in predicting a unique vector solution of these 3 parameters. Therefore, it is essential to define a combination of the output parameters based on physical principles. The physic-based proposed combination leading to the energy reads:

$$E = t \times (P_{HF} + P_{MF}) \quad (8)$$

However, it is known that the tooth tip and the tooth root are influenced by the high and medium frequencies of the process, respectively [64–66]. The generators work simultaneously under the same heating time; hence, it is possible to consider the problem based on the specific location in the gear in order to obtain more information about the different process parameters such as:

$$\begin{aligned} E_{HF} &= t \times P_{HF} \\ E_{MF} &= t \times P_{MF} \end{aligned} \quad (9)$$

Hence, the inverse problem defined in Equation (7) can be expressed as:

$$\begin{aligned} f(H_{t,0}, H_{t,08}, H_{t,1}, H_{t,2}, H_{t,3}) &= E_{HF} \\ f(H_{r,0}, H_{r,08}, H_{r,1}, H_{r,2}, H_{r,3}) &= E_{MF} \end{aligned} \quad (10)$$

where H_t and H_r are the hardness measured at the tooth tip and tooth root, respectively.

Finally, the initial inverse modeling is reduced to a simple regression problem. The tested algorithms and results are presented in the next section.

4. Inverse Modeling and Results

The modeling was divided into two stages. First, data were used in several machine learning techniques and tested to evaluate the best algorithm. These algorithms vary from complex such as XGBoost to multi-linear regression. It is important to use quite simple algorithms when it is possible to save computational time. Second, the results of the inverse model were used in the forward problem for validation purpose.

4.1. Inverse Modeling

The dataset was composed of 60 runs (30 runs in both, the tooth root and tooth tip). It is worth mentioning that 70% of the dataset was considered for training, and 30% for test. As mentioned above, different models were selected to predict the energy such as XGBoost regressor [67], Random Forest (RF) [68,69], Multi-linear regression [70], and Support Vector Regressor (SVR) [71,72].

The obtained results listed in Table 3 show a satisfying performance for each model as the error is relatively low (<10%). It suggests that the inverse problem is now properly defined.

Table 3. Test results for inverse modeling.

Position	Error	XGBoost	Random Forest	Multi-Linear Regression	SVR
Tooth tip	RMSE	1.07	1.42	0.74	1.34
	RMSPE	5.78%	7.23%	3.71%	7.99%
Tooth root	RMSE	0.84	2.58	0.78	2.27
	RMSPE	4.53%	6.78%	3.93%	5.65%

The characteristic hardness measurements chosen for variables are meaningful according to the promising obtained results. As the error differs depending on the data that are randomly put in training and testing during the split, the selection of the data was optimized with respect to test results. However, cross-validation technique [73] was used to ensure the robustness of the model but is unstable because of the small number of samples [74,75]. With this amount of data, the presented models cannot be generalized. Results from multi-linear regression model were illustrated in Figure 5.

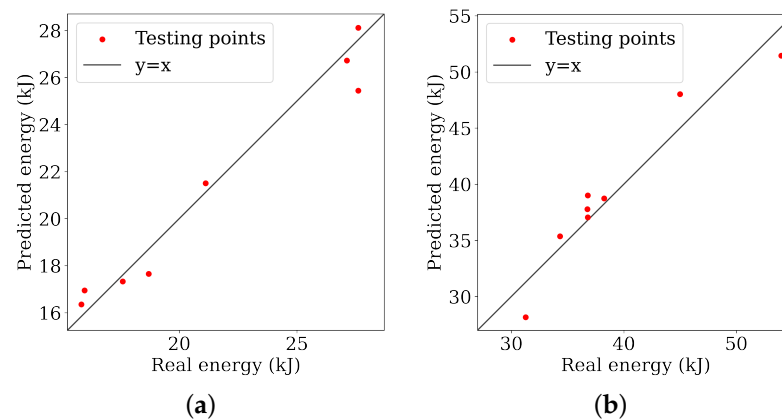


Figure 5. Predicted versus real energy at the tooth tip and the tooth root. (a) Tooth tip; (b) Tooth root.

It is worth noticing that the data are well predicted within the fixed ranges of energy. Moreover, these results show that a simple algorithm such as multi-linear regression can handle the simplified problem.

4.2. Forward Problem Consistency

In order to ensure that it is possible to turn back to the forward problem with the available variables presented in the previous section, the next step of this work is to predict the hardness with the previous output parameters i.e., the energy. The problem could be expressed as:

$$\begin{aligned} f(E_{MF}) &= (H_0, H_{08}, H_1, H_2, H_3) \\ f(E_{HF}) &= (H_0, H_{08}, H_1, H_2, H_3) \end{aligned} \quad (11)$$

Predicting multiple outputs with one variable as input is fairly complex in regression especially when the variables are dependent on each other. Since the hardness points $(H_0, H_{08}, H_1, H_2, H_3)$ were selected from fixed depth to keep the data homogeneity, it is possible to divide the hardness and depth into 2 variables. The depth being known, it can be considered as an input variable.

Hence the input space of the variables could be written as :

$$X = \{E, loc, d\} \quad (12)$$

where E is the energy of the location of the point, loc is the location, either the root or tip of the tooth, and d is the depth of the measured hardness. Therefore, the problem is such as:

$$f(E, d, loc) = H \quad (13)$$

There are some differences between the inverse and forward approaches. The location in the gear is now considered as the input variable loc . Contrary to the inverse approach using one model per location, in the forward problem the locations are encoded and only one model is needed. In addition, in the inverse problem, one instance represents a hardness profile, while in the forward problem, an instance is now a single hardness measurement linked to its depth. Because of this difference and to ensure consistency of the profiles while splitting for training and testing sets, the data are split according to their respective profile. Therefore, 24 profiles were considered for training, leaving seven profiles for the testing phase. The results of the four models for the forward approach show fairly different errors from misprediction to promising results. They are listed in Table 4.

Table 4. Test results of the hardness prediction.

Error	XGBoost	Multi-Linear Regression	Random Forest	SVR
RMSE	45.55	134.25	47.15	137.59
RMSPE	8.5%	28.75%	9.2%	37.26%

It is clear that the XGBoost and Random Forest algorithms comparatively give a much better prediction of the hardness. The best models are illustrated in Figure 6. Bulk and surface hardness (≈ 300 HV and 700 HV) are well predicted, while both models showed difficulties when predicting hardness in the transition phase (between surface and core hardness). This difficulty can be explained by several factors.

Indeed, the problem is already complex, and the number of samples used is fairly low. Moreover, the variables are limited to those that have already been used in the inverse problem. However, it is known that the surface and in-depth temperatures [44] or the austenite ratio [38] can highly increase the accuracy of the hardness prediction in the transition zone. Beyond this method, such variables could be used to enhance the efficiency of the model.

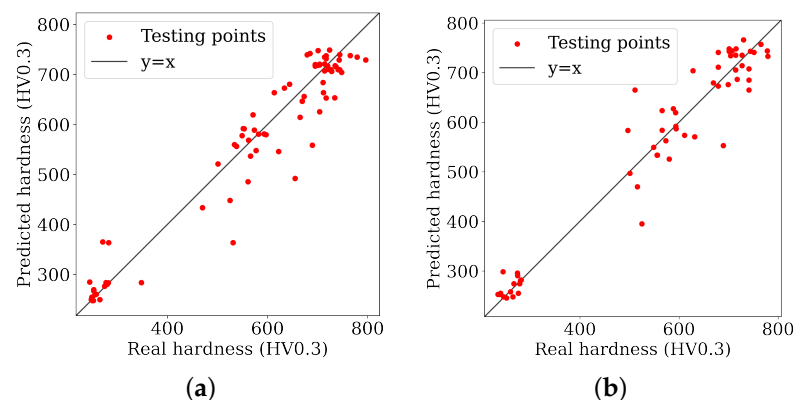


Figure 6. Predicted versus real hardness for forward problem in both tooth tip and root of the gear. (a) Random Forest; (b) XGBoost.

5. Conclusions

This work proposed an inverse approach of the hardness. Data were collected from induction hardening experiments carried out on C45 spur-gear. In this work, an inverse modeling based on machine learning was presented. This method consists of predicting process parameters of induction hardening treatment based on the hardness profiles. The method proceeded by discretizing the profiles, the combination of the process parameters, and the forward problem-based verification. The main conclusions were as follows:

- The discretization of hardness profile and the physics-based combination of the output variables of the data were essential to conduct the inverse modeling.
- It was shown that simple algorithms were efficient to predict the energy.
- The number of available samples was too small to prove the generalization of the model.
- The results of the forward problem verification proved the efficiency of the proposed approach.

It is worth outlining that the inverse approach model has the advantage to be simple and easy to conduct with no data shape issues. In addition, the developed method have the advantages of a shorter time response than complex inverse methods which is highly suitable for process optimization. In the light of the results, the proposed inverse approach can be used in induction hardening optimization.

Author Contributions: Conceptualization, F.C.; methodology, S.G.; software, S.G.; supervision, M.D. and F.C. writing—original draft preparation, S.G.; writing—review and editing, M.D. and F.C. All authors have read and agreed to the published version of the manuscript.

Funding: This research was carried out as part of a project TRANSFUGE sponsored by the french institute of research and technology in materials, metallurgy and processes (IRT M2P), France. The project benefited from funding from a consortium of industrial partners and the French PIA (Plan d'Investissement d'Avenir) granted the French National Agency for Research (ANR).

Data Availability Statement: Provided under request.

Acknowledgments: This work was conducted with the help of the French Technological Research Institute for Materials, Metallurgy and Processes (IRT M2P). The authors would like to acknowledge IRT M2P and the partners of the project TRANSFUGE led by IRT M2P.

Conflicts of Interest: The authors declare no conflict of interest.

References

1. Rokicki, P. Induction hardening of tool steel for heavily loaded aircraft engine components. *Arch. Metall. Mater.* **2017**, *62*, 315–320. [[CrossRef](#)]
2. Candeo, A.; Ducassy, C.; Bocher, P.; Dughiero, F. Multiphysics Modeling of Induction Hardening of Ring Gears for the Aerospace Industry. *IEEE Trans. Magn.* **2011**, *47*, 918–921. [[CrossRef](#)]
3. Rudnev, V.; Loveless, D.; Cook, R. *Handbook of Induction Heating*, 2nd ed.; CRC Press: Boca Raton, FL, USA, 2017.
4. Qiu, G.; Zhan, D.; Li, C.; Yang, Y.; Qi, M.; Jiang, Z.; Zhang, H. Effects of yttrium and heat treatment on the microstructure and mechanical properties of CLAM steel. *J. Mater. Eng. Perform.* **2020**, *29*, 42–52. [[CrossRef](#)]
5. Celada-Casero, C.; Huang, B.; Yang, J.R.; San-Martin, D. Microstructural mechanisms controlling the mechanical behaviour of ultrafine grained martensite/austenite microstructures in a metastable stainless steel. *Mater. Des.* **2019**, *181*, 107922. [[CrossRef](#)]
6. Zhong, H.; Wang, Z.; Gan, J.; Wang, X.; Yang, Y.; He, J.; Wei, T.; Qin, X. Numerical simulation of martensitic transformation plasticity of 42CrMo steel based on spot continual induction hardening model. *Surf. Coat. Technol.* **2020**, *385*, 125428. [[CrossRef](#)]
7. Hömberg, D.; Liu, Q.; Montalvo-Urquizo, J.; Nadolski, D.; Petzold, T.; Schmidt, A.; Schulz, A. Simulation of multi-frequency-induction-hardening including phase transitions and mechanical effects. *Finite Elem. Anal. Des.* **2016**, *121*, 86–100. [[CrossRef](#)]
8. Yoshida, W. Residual stress control on bearing steel by surface cooled induction heating fast tempering. *J. Mater. Eng. Perform.* **2020**, *29*, 3585–3592. [[CrossRef](#)]
9. Li, F.; Li, X.; Wang, T.; Rong, Y.K.; Liang, S.Y. In-process residual stresses regulation during grinding through induction heating with magnetic flux concentrator. *Int. J. Mech. Sci.* **2020**, *172*, 105393. [[CrossRef](#)]
10. Maresca, F.; Kouznetsova, V.; Geers, M.; Curtin, W. Contribution of austenite-martensite transformation to deformability of advanced high strength steels: From atomistic mechanisms to microstructural response. *Acta Mater.* **2018**, *156*, 463–478. [[CrossRef](#)]
11. Xu, S.; Li, J.; Cui, Y.; Zhang, Y.; Sun, L.; Li, J.; Luan, J.; Jiao, Z.; Wang, X.L.; Liu, C.; et al. Mechanical properties and deformation mechanisms of a novel austenite-martensite dual phase steel. *Int. J. Plast.* **2020**, *128*, 102677. [[CrossRef](#)]

12. Li, Z.; Ferguson, B.L. Controlling gear distortion and residual stresses during induction hardening. *Gear Technol.* **2012**. Available online: <https://www.geartechnology.com/ext/resources/issues/0312x/ferguson.pdf> (accessed on 18 April 2023).
13. Nemkov, V.; Goldstein, R.; Jackowski, J.; Ferguson, L.; Li, Z. Stress and distortion evolution during induction case hardening of tube. *J. Mater. Eng. Perform.* **2013**, *22*, 1826–1832. [[CrossRef](#)]
14. Areitioaurtena, M.; Segurajauregi, U.; Urresti, I.; Fisk, M.; Ukar, E. Predicting the induction hardened case in 42CrMo4 cylinders. *Procedia CIRP* **2020**, *87*, 545–550. [[CrossRef](#)]
15. Kabanikhin, S.I. Definitions and examples of inverse and ill-posed problems. *J. Inverse Ill-Posed Probl.* **2008**, *16*, 317–357. [[CrossRef](#)]
16. Pizlo, Z. Perception viewed as an inverse problem. *Vis. Res.* **2001**, *41*, 3145–3161. [[CrossRef](#)] [[PubMed](#)]
17. Mohamad-Djafari, A. *Inverse Problems in Vision and 3D Tomography*; John Wiley & Sons: Hoboken, NJ, USA, 2013.
18. Bertero, M.; Boccacci, P.; De Mol, C. *Introduction to Inverse Problems in Imaging*; CRC Press: Boca Raton, FL, USA, 2021.
19. McCann, M.T.; Jin, K.H.; Unser, M. Convolutional neural networks for inverse problems in imaging: A review. *IEEE Signal Process. Mag.* **2017**, *34*, 85–95. [[CrossRef](#)]
20. Ongie, G.; Jalal, A.; Metzler, C.A.; Baraniuk, R.G.; Dimakis, A.G.; Willett, R. Deep learning techniques for inverse problems in imaging. *IEEE J. Sel. Areas Inf. Theory* **2020**, *1*, 39–56. [[CrossRef](#)]
21. Gladwell, G.M. *Inverse Problems in Vibration*; Springer: Berlin/Heidelberg, Germany, 1986.
22. Egbert, G.D.; Kelbert, A. Computational recipes for electromagnetic inverse problems. *Geophys. J. Int.* **2012**, *189*, 251–267. [[CrossRef](#)]
23. MacLeod, R.S.; Brooks, D.H. Recent progress in inverse problems in electrocardiology. *IEEE Eng. Med. Biol. Mag.* **1998**, *17*, 73–83. [[CrossRef](#)]
24. McCann, M.T.; Unser, M. Biomedical image reconstruction: From the foundations to deep neural networks. *Found. Trends[®] Signal Process.* **2019**, *13*, 283–359. [[CrossRef](#)]
25. Sun, N.Z. *Inverse Problems in Groundwater Modeling*; Springer: Berlin/Heidelberg, Germany, 2013; Volume 6.
26. De Vito, E.; Rosasco, L.; Caponnetto, A.; De Giovannini, U.; Odone, F.; Bartlett, P. Learning from Examples as an Inverse Problem. *J. Mach. Learn. Res.* **2005**, *6*, 883–904.
27. Arridge, S.; Maass, P.; Öktem, O.; Schönlieb, C.B. Solving inverse problems using data-driven models. *Acta Numer.* **2019**, *28*, 1–174. [[CrossRef](#)]
28. Vieweg, A.; Ressel, G.; Prevedel, P.; Raninger, P.; Panzenböck, M.; Marsoner, S.; Ebner, R. Induction hardening: Differences to a conventional heat treatment process and optimization of its parameters. *Proc. IOP Conf. Ser. Mater. Sci. Eng.* **2016**, *119*, 012019. [[CrossRef](#)]
29. Xu, D.h.; Kuang, Z.B. A study on the distribution of residual stress due to surface induction hardening. *J. Eng. Mater. Technol.* **1996**, *118*, 571–575. [[CrossRef](#)]
30. Choi, J.K.; Park, K.S.; Lee, S.S. Prediction of high-frequency induction hardening depth of an AISI 1045 specimen by finite element analysis and experiments. *Int. J. Precis. Eng. Manuf.* **2018**, *19*, 1821–1827. [[CrossRef](#)]
31. Muhammad, M.; Siddiqui, M.A.; Muhammad, S. Experimental investigation and optimization of process parameters for through induction hardening using factorial design of experiments. *J. Eng. Res.* **2017**, *5*, 174–185.
32. Misra, M.K.; Bhattacharya, B.; Singh, O.; Chatterjee, A. Multi response optimization of induction hardening process—a new approach. *IFAC Proc. Vol.* **2014**, *47*, 862–869. [[CrossRef](#)]
33. Kaiser, D.; Damon, J.; Mühl, F.; de Graaff, B.; Kiefer, D.; Dietrich, S.; Schulze, V. Experimental investigation and finite-element modeling of the short-time induction quench-and-temper process of AISI 4140. *J. Mater. Process. Technol.* **2020**, *279*, 116485. [[CrossRef](#)]
34. Zhou, H.; Zhao, D.; Liu, Y.; Li, G. Influence of Induction Hardening Process on Camshafts' Residual Stresses. *Arab. J. Sci. Eng.* **2020**, *45*, 9651–9659. [[CrossRef](#)]
35. Javaheri, V.; Asperheim, J.I.; Grande, B.; Kolli, S.; Porter, D. Simulation and experimental studies of induction hardening behavior of a new medium-carbon, low-alloy wear resistance steel. *COMPEL Int. J. Comput. Math. Electr. Electron. Eng.* **2020**. [[CrossRef](#)]
36. Hutton, D.V. *Fundamentals of Finite Element Analysis*; McGraw-Hill Science Engineering: Columbus, OH, USA, 2003.
37. Guo, Y.; Liu, M.; Yan, Y. Hardness Prediction of Grind-Hardening Layer Based on Integrated Approach of Finite Element and Cellular Automata. *Materials* **2021**, *14*, 5651. [[CrossRef](#)] [[PubMed](#)]
38. Derouiche, K.; Garois, S.; Champaney, V.; Daoud, M.; Traidi, K.; Chinesta, F. Data-Driven Modeling for Multiphysics Parametrized Problems—Application to Induction Hardening Process. *Metals* **2021**, *11*, 738. [[CrossRef](#)]
39. Zhang, Y.; Ruan, J.; Huang, T.; Yang, X.; Zhu, H.; Yang, G. Calculation of temperature rise in air-cooled induction motors through 3-D coupled electromagnetic fluid-dynamical and thermal finite-element analysis. *IEEE Trans. Magn.* **2012**, *48*, 1047–1050. [[CrossRef](#)]
40. Javaheri, V.; Pohjonen, A.; Asperheim, J.I.; Ivanov, D.; Porter, D. Physically based modeling, characterization and design of an induction hardening process for a new slurry pipeline steel. *Mater. Des.* **2019**, *182*, 108047. [[CrossRef](#)]
41. Daoud, M.; Kubler, R.; Bemou, A.; Osmond, P.; Polette, A. Prediction of residual stress fields after shot-peening of TRIP780 steel with second-order and artificial neural network models based on multi-impact finite element simulations. *J. Manuf. Process.* **2021**, *72*, 529–543. [[CrossRef](#)]
42. Fisk, M.; Lindgren, L.E.; Datchary, W.; Deshmukh, V. Modelling of induction hardening in low alloy steels. *Finite Elem. Anal. Des.* **2018**, *144*, 61–75. [[CrossRef](#)]

43. Mühl, F.; Damon, J.; Dietrich, S.; Schulze, V. Simulation of induction hardening: Simulative sensitivity analysis with respect to material parameters and the surface layer state. *Comput. Mater. Sci.* **2020**, *184*, 109916. [[CrossRef](#)]
44. Garois, S.; Daoud, M.; Traidi, K.; Chinesta, F. Artificial intelligence modeling of induction contour hardening of 300M steel bar and C45 steel spur-gear. *Int. J. Mater. Form.* **2023**, submitted. [[CrossRef](#)]
45. Wu, J.; Xu, Z.; Qiao, H.; Zhao, J.; Huang, Z. Mechanical properties prediction of superalloy FGH4095 treated by laser shock processing based on machine learning. *Mater. Lett.* **2021**, *297*, 129970. [[CrossRef](#)]
46. Krause, C.; Uysal, B.; Engler, M.; Radek, C.; Schaudig, M. Application of Machine Learning Techniques to Determine Surface Hardness Based on the Barkhausen Effect. *HTM J. Heat Treat. Mater.* **2022**, *77*, 409–424. [[CrossRef](#)]
47. Asadzadeh, M.Z.; Raninger, P.; Prevedel, P.; Ecker, W.; Mücke, M. Inverse model for the control of induction heat treatments. *Materials* **2019**, *12*, 2826. [[CrossRef](#)] [[PubMed](#)]
48. Nguyen, K.T.; Bendada, A. An inverse approach for the prediction of the temperature evolution during induction heating of a semi-solid casting billet. *Model. Simul. Mater. Sci. Eng.* **2000**, *8*, 857. [[CrossRef](#)]
49. Byrne, C.L. *Iterative Optimization in Inverse Problems*; CRC Press: Boca Raton, FL, USA, 2014.
50. Ye, N.; Roosta-Khorasani, F.; Cui, T. Optimization methods for inverse problems. *2017 MATRIX Ann.* **2019**, *2*, 121–140.
51. Peyré, G.; Bougleux, S.; Cohen, L. Non-local regularization of inverse problems. In Proceedings of the Computer Vision–ECCV 2008: 10th European Conference on Computer Vision, Marseille, France, 12–18 October 2008; Proceedings, Part III 10; Springer: Berlin/Heidelberg, Germany, 2008; pp. 57–68.
52. Egger, H.; Engl, H.W. Tikhonov regularization applied to the inverse problem of option pricing: Convergence analysis and rates. *Inverse Probl.* **2005**, *21*, 1027. [[CrossRef](#)]
53. Benning, M.; Burger, M. Modern regularization methods for inverse problems. *Acta Numer.* **2018**, *27*, 1–111. [[CrossRef](#)]
54. Calvetti, D.; Somersalo, E. Inverse problems: From regularization to Bayesian inference. *Wiley Interdiscip. Rev. Comput. Stat.* **2018**, *10*, e1427. [[CrossRef](#)]
55. Schmidt, D.M.; George, J.S.; Wood, C.C. Bayesian inference applied to the electromagnetic inverse problem. *Hum. Brain Mapp.* **1999**, *7*, 195–212. [[CrossRef](#)]
56. Ma, X.; Zabaras, N. An efficient Bayesian inference approach to inverse problems based on an adaptive sparse grid collocation method. *Inverse Probl.* **2009**, *25*, 035013. [[CrossRef](#)]
57. Sridharan, B.; Goel, M.; Priyakumar, U.D. Modern machine learning for tackling inverse problems in chemistry: Molecular design to realization. *Chem. Commun.* **2022**, *58*, 5316–5331. [[CrossRef](#)]
58. Pillozzi, L.; Farrelly, F.A.; Marcucci, G.; Conti, C. Machine learning inverse problem for topological photonics. *Commun. Phys.* **2018**, *1*, 57. [[CrossRef](#)]
59. *EN ISO 6507-1: 2018; Metallic Materials—Vickers Hardness Test—Part 1: Test Method.* ISO: Geneva, Switzerland, 2018.
60. Duda, R.O.; Hart, P.E. *Pattern Classification and Scene Analysis*; John Wiley & Sons: Hoboken, NJ, USA, 1973; Volume 3.
61. Gareth, J.; Daniela, W.; Trevor, H.; Robert, T. *An Introduction to Statistical Learning: With Applications in R*; Springer: Berlin/Heidelberg, Germany, 2013.
62. Kubat, M. Neural networks: A comprehensive foundation by Simon Haykin, Macmillan, 1994, ISBN 0-02-352781-7. *Knowl. Eng. Rev.* **1999**, *13*, 409–412. [[CrossRef](#)]
63. Labach, A.; Salehinejad, H.; Valaee, S. Survey of dropout methods for deep neural networks. *arXiv* **2019**, arXiv:1904.13310.
64. Al Salkhadi, A.A.M. Modélisation et Simulation du Procédé de Durcissement par Induction Appliqué à des Pignons à Chaîne-Chauffage à Double Fréquence. Ph.D. Thesis, Université du Québec à Rimouski, Rimouski, QC, Canada, 2021.
65. Barglik, J.; Smagór, A.; Smalcerz, A.; Desisa, D.G. Induction Heating of Gear Wheels in Consecutive Contour Hardening Process. *Energies* **2021**, *14*, 3885. [[CrossRef](#)]
66. Zhao, Y.Q.; Han, Y.; Xiao, Y. An asynchronous dual-frequency induction heating process for bevel gears. *Appl. Therm. Eng.* **2020**, *169*, 114981. [[CrossRef](#)]
67. Chen, T.; Guestrin, C.; XGBoost: A Scalable Tree Boosting System. In Proceedings of the 22nd ACM SIGKDD International Conference on Knowledge Discovery and Data Mining (KDD '16), San Francisco, CA, USA, 13–17 August 2016; Association for Computing Machinery: New York, NY, USA, 2016; pp. 785–794. [[CrossRef](#)]
68. Breiman, L. Random forests. *Mach. Learn.* **2001**, *45*, 5–32. [[CrossRef](#)]
69. Cutler, A.; Cutler, D.R.; Stevens, J.R. Random forests. In *Ensemble Machine Learning: Methods and Applications*; Springer: New York, NY, USA, 2012; pp. 157–175.
70. Bottenberg, R.A.; Ward, J.H. *Applied Multiple Linear Regression*; 6570th Personnel Research Laboratory, Aerospace Medical Division, Air Force: San Antonio, TX, USA, 1963; Volume 63.
71. Smola, A.J.; Schölkopf, B. A tutorial on support vector regression. *Stat. Comput.* **2004**, *14*, 199–222. [[CrossRef](#)]
72. Awad, M.; Khanna, R.; Awad, M.; Khanna, R. Support vector regression. In *Efficient Learning Machines: Theories, Concepts, and Applications for Engineers and System Designers*; Springer: Berlin/Heidelberg, Germany, 2015; pp. 67–80.
73. Santos, M.S.; Soares, J.P.; Abreu, P.H.; Araujo, H.; Santos, J. Cross-Validation for Imbalanced Datasets: Avoiding Overoptimistic and Overfitting Approaches [Research Frontier]. *IEEE Comput. Intell. Mag.* **2018**, *13*, 59–76. [[CrossRef](#)]

74. Rao, R.B.; Fung, G.; Rosales, R. On the dangers of cross-validation. An experimental evaluation. In Proceedings of the 2008 SIAM International Conference on Data Mining, Alexandria, VA, USA, 28–30 April 2008; SIAM: Philadelphia, PA, USA, 2008; pp. 588–596.
75. Isaksson, A.; Wallman, M.; Göransson, H.; Gustafsson, M.G. Cross-validation and bootstrapping are unreliable in small sample classification. *Pattern Recognit. Lett.* **2008**, *29*, 1960–1965. [[CrossRef](#)]

Disclaimer/Publisher’s Note: The statements, opinions and data contained in all publications are solely those of the individual author(s) and contributor(s) and not of MDPI and/or the editor(s). MDPI and/or the editor(s) disclaim responsibility for any injury to people or property resulting from any ideas, methods, instructions or products referred to in the content.